Study of the Key Technology of Ghost Imaging Based on Rosette Scanning

Zhang Leihong[1], Kang Yi[1]*, Pan Zilan[1], Liang Dong[1], Li Bei[1], Zhang Dawei[1], and Ma Xiuhua[2]

[1]*University of Shanghai for Science and Technology, Shanghai 200093, China*
[2]*Shanghai Institute of Optics and Fine Mechanics, CAS, Shanghai 201800, China*

Ghost imaging offers great potential, with respect to standard imaging, for imaging objects in optically harsh or noisy environments. It can solve the problems that are difficult to solve by conventional imaging techniques. Recently, it has become a hot topic in quantum optics. In this paper, we propose a scheme for ghost imaging based on rosette scanning, named *rosette ghost imaging*. Sampling a small area sampling instead of the whole object, the instantaneous field of view of rosette scanning is used as the modulation light field in ghost imaging. This scheme reduces energy loss, the number of samples, and the sampling time, while improving the quality of the reconstructed image.

Keywords : Ghost imaging, Rosette scanning, Instantaneous field of view, Image reconstruction
OCIS codes : (100.3010) Image reconstruction techniques; (110.2990) Image formation theory

I. INTRODUCTION

Recently, ghost imaging (GI) has become a hot topic in quantum optics [1]. Ghost imaging offers great potential, with respect to standard imaging, for imaging objects in optically harsh or noisy environments. The earliest GI experiment was achieved on the basis of entangled photon pairs. The theory of entangled photon pairs was proposed by Klyshko [2]. Subsequent experiments and theories proved that an entangled light source is not an essential condition for GI; a classical, thermal light source also can realize GI [3]. Subsequently, GI based on a thermal light source has promoted many new studies, and has gradually progressed from theory to experiment and practical application. Paper [4] studied the applications of GI based on a thermal light source, and the influence of noise on GI. Paper [5] improved the imaging principle and imaging device of GI based on a thermal light source. Paper [6] used a real thermal light field to realize GI without an optical lens. In addition, Paper [7] studied high-order GI and pure-phase-object GI. Paper [8] combined an information-theory method with GI. In the experimental aspect, second-order GI of a scattering medium was successfully conducted in paper [9]. Paper [10] used only one detector to achieve a successful experiment on GI

based on a pseudothermal light source. Paper [11] proposed computational ghost imaging, reduced the complexity of the experiment and improved its efficiency. Paper [12] improved the algorithm for second-order GI and proposed differential ghost imaging.

A rosette scanning seeker is a type of single infrared (IR) detector [13]. A rosette scanning system uses a fixed instantaneous field of view (IFOV) to scan the total field of view (TFOV), detects the target location and image information, and then restores the detected information through a variety of processing methods. It has important application value and is a low-cost infrared homing technology. Paper [14] proposed a method to design a small IFOV without lessening the TFOV, to solve the problem that the previous method could not achieve full scan coverage, but accurate imaging of objects in a harsh environment was still a question. In paper [15], the information from a single-detector rosette scanning system was used with compressive sensing to reconstruct the image, and work efficiency was improved. However, as a receiving device, the detector is easily influenced by the light source, and other factors. In this paper we propose a scheme for ghost imaging based on rosette scanning, named *rosette ghost imaging* (RGI). RGI combines ghost imaging and a rosette

---

scanning system; the IFOV of rosette scanning, which collects partial information about the object each time, is used as the modulated light field for GI. Using this method to detect the object, laser energy is relatively concentrated, because the detection range is small. The overall effect is better than that of GI, and RGI improves the signal-to-noise ratio while reducing the number of samples and sampling time.

II. THEORY OF GHOST IMAGING AND ROSETTE SCANNING

2.1. Ghost Imaging

In computational ghost imaging, a laser irradiates a spatial light modulator (SLM), which modulates the laser's intensity. The modulated light field then irradiates the object. A bucket detector collects all light passing through the object, and a bucket detector value is obtained. Each value is related to the transmission function of the object. In the following formula, $T(x, y)$ is the transmission function of the object.

$$D_i = \int T(x, y) I_i(x, y) dx dy \quad (i = 1, 2 \cdots N) \tag{1}$$

After N samples, the N bucket detector values D_i are obtained, and the speckle field $I_i(x, y)$ generated by the SLM for each modulation is recorded. The second-order correlation function is obtained by correlating the speckle-field intensity distribution I and bucket detector values D. In the following formula, where $\langle\ \rangle$ represents arithmetic mean, $G(x, y)$ represents the image of the target object.

$$G(x, y) = \langle I_i(x, y) D_i \rangle - \langle I_i(x, y) \rangle \langle D_i \rangle \quad i = 1, 2 \cdots N \tag{2}$$

Figure 1 is a schematic diagram for computational ghost imaging.

2.2. Rosette Scanning

In a rosette scanning system, a detector unit with a small instantaneous field of view (IFOV), scanning in a rosette pattern generated by two oppositely rotated optical deflectors, is used to detect a thermal radiation target. Figure 2 is a schematic diagram of a rosette scanning
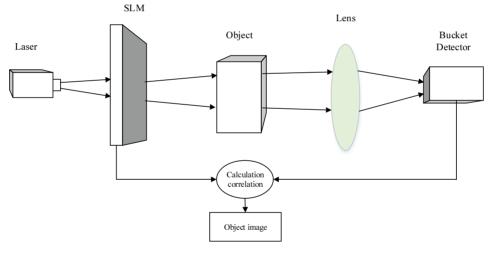

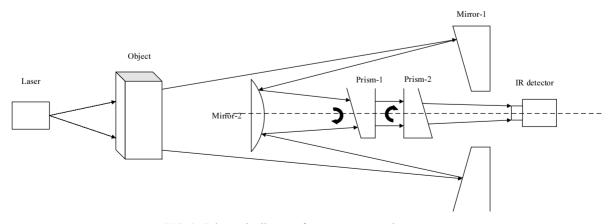FIG. 1. Schematic diagram for computational ghost imaging.

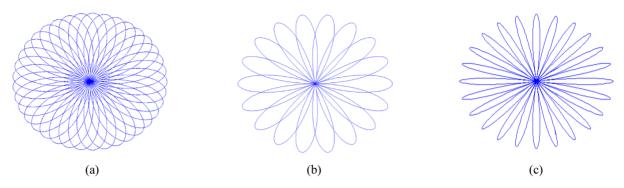FIG. 2. Schematic diagram for a rosette scanning system.

FIG. 3. Rosette scanning patterns for different frequencies: (a) f_1 = 150, f_2 = 72; (b) f_1 = 275, f_2 = 175; (c) f_1 = 130, f_2 = 110.

system. The rotation frequency of the eccentric lens is f_1, and the rotation frequency of the secondary mirror installed on the gyro is f_2. Different values of f_1 and f_2 produce different scanning patterns, as shown as Fig. 3. The locus of the pattern can be derived as follows:

$$x(t) = \frac{\rho}{2}(\cos(2\pi f_1 t) + \cos(2\pi f_2 t))$$
$$y(t) = \frac{\rho}{2}(\sin(2\pi f_1 t) - \sin(2\pi f_2 t))$$

(3)

where ρ is the half angle of the TFOV of the seeker, and determines the size of the TFOV.

The rotating frequencies f_1 and f_2 of two prisms determine the scanning speed and rosette shape. f is the greatest common divisor of f_1 and f_2, $N_1 = f_1 / f$, $N_2 = f_2 / f$; when N_1 and N_2 are positive integers, a closed pattern is formed by scanning. The rosette scanning system completes one scan in $T = 1/f$ s. The number of petals is computed as $N = N_1 + N_2 = \frac{f_1 + f_2}{f}$.

The number of petals N determines the size of the IFOV. The width of each petal increases with the increase in N ($N = N_1 - N_2$). The petals will not overlap when $N < 3$, as shown as Fig. 3(c). When the target object is not in the center of the field of view (FOV), the pulse form lacks periodicity, but according to the relationship between pulse and time, if the pulse generation time has been recorded, the coordinate of the target is calculated by the trajectory equation for rosette scanning. The object is scanned by fixed IFOV in a rosette scanning system. The IFOV is small, but its constraint is that the IFOV should cover the TFOV after one scan period. Therefore, the relationship between IFOV and TFOV needs to be established. The size of the IFOV is

$$\omega = \frac{2\pi}{N}\rho\cos(\pi/\Delta N)$$

(4)

As Fig. 4 shows, the scope of the TFOV is roughly circular, the IFOV passes through the central frequency far more than the edge, and the central part scanned by IFOV
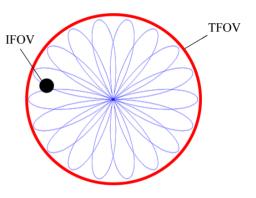

FIG. 4. IFOV and TFOV of a rosette scanning pattern.

has overlap, but the marginal part has clearance. In the process of sampling, the sampling density of the center is much greater than that of the margin. When the number of petals increases, as shown as Fig. 3(a), the scanning track is intensive, the area of overlap is increased, and the coverage of the marginal area is more extensive. At the same time, many issues appear with it: The scanning period and number of samples are increased.

The center of the IFOV can be calculated using Eq. (3), the coordinate of the object can be calculated using the trajectory equation for rosette scanning at the end of one scan cycle, and the location of the target can be determined [15]. If we want to obtain information about the shape of the object, the sampling points in one scanning cycle can be mapped to a two-dimensional space in turn. If the location detects a target, its value is 1, otherwise its value is 0. The real shape of the target can be obtained by mapping different classes of points back into the scan space [16].

III. THEORY OF GHOST IMAGING BASED ON ROSETTE SCANNING

In traditional GI, a laser modulated by an SLM irradiates an object, the modulated light field covering whole object. However, the large light field leads to dispersion of the laser's energy. In a rosette scanning system, the object is

scanned by a smaller IFOV in every sampling, and the object's information can be obtained after one scan period. The range of the IFOV is small; the area sampled every time is small, so the laser energy is concentrated.

When rosette scanning is used for ghost imaging, the IFOV of rosette scanning is used to replace the light field of GI, which is modulated by an SLM to sample the information of the scene. The IFOV samples the scene's information, so the range that is sampled by RGI is small and the laser's energy is more concentrated, so the energy of sampled image information that is collected by the bucket detector is much greater than with a traditional method, and the image can be sampled completely after one scan period. Compared to GI, RGI uses a small light field to replace a large light filed, concentrated energy replaces dispersed energy, and the sampling effect is improved.

RGI uses an IFOV to sample object information; the smaller the IFOV, the higher the anti-interference ability and the more the energy is concentrated, but the TFOV will become smaller, and the sampled image information incomplete. Therefore, the size of IFOV needs to be determined, and it is important to balance TFOV and IFOV. The size of the IFOV can be calculated with Eq. (4), and this IFOV collects object information along the rose line,

so that there will be no void but there will be overlap in the TFOV. In fact, Eq. (4) applies only when $\Delta N > 3$. When ΔN is larger, the IFOV will also increase, and the overlap as well. From a practical consideration, generally $\Delta N \geq 7$, the void of the object can be ignored.

In a GI system, a laser modulated by an SLM irradiates the object, and a bucket detector obtains a bucket detector value; this is one sampling. In RGI, to convert between Hz and sampling number, sample once every 0.1 ms. A rosette scanning pattern is constructed, $f_1 = 275 Hz$, $f_2 = 175 Hz$; a rosette scanning cycle is 0.04 s long, and the sampling number of a rosette scanning cycle is 400. As shown as Fig. 5(b), a point represents the location of one IFOV center. The region of the IFOV is shown in Fig. 5(c). The test image is shown in Fig. 5(a), and the image in Fig. 5(d), which is a part of test image, is sampled by IFOV. RGI uses IFOV to sample a scene and obtain a bucket detector value. The IFOV is not a single point but rather a small circular region, as shown in Fig. 5(c). Every sampling includes information that is sampled by IFOV; the sampled information is part of the whole scene, as shown in Fig. 5(d). Every sampling is part of the scene, so sampling of a scene can be regarded as a collection of multiple IFOV.

In the process of sampling, the object's information is

(a)   (b)   (c)   (d)
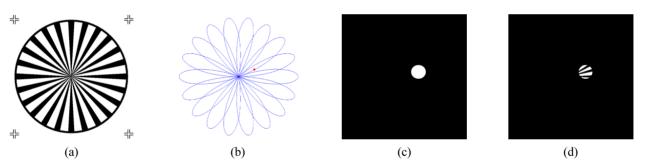
FIG. 5. (a) The test image, (b) the rosette scanning pattern, (c) the IFOV region, and (d) the samples obtained from the test image for a given IFOV location.
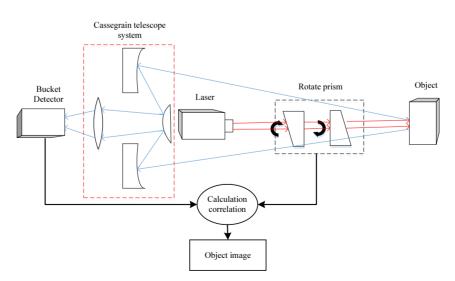

FIG. 6. Schematic diagram for RGI.

collected by suitable IFOV. The intensity distribution of IFOV $I(x,y)$ takes the place of the light field in GI. In the ith collection process, IFOV $I(x,y)$ that passes through the object is received by the bucket detector, and a bucket detector value D_i is obtained D_i via Eq. (1). The bucket detector obtains many values after one cycle of sampling, the average of which is $<D_i>$, and the average of the intensity distribution of the IFOV is $<I_i(x,y)>$. The second-order correlation function is found by a correlating operation for the intensity distribution of the IFOV and bucket detector values, as shown in Eq. (2). The result $G(x,y)$ is the object image reconstructed by RGI.

The Fig. 6 is a schematic diagram of RGI.

IV. SIMULATION OF RGI

The performance of RGI is verified through numerical simulations. To facilitate the simulations, the test images are from the MATLAB image library, in which a standard image is the "Lena" image; the size of the image is set to 80×80 pixels. The rotating frequencies of the optical elements are $f_1 = 160 Hz$ and $f_2 = 70 Hz$ respectively, a rosette scanning cycle is 0.1 s long, and the number of samples for a cycle is 1000. The radius of TFOV is 40 pixels. The size of the IFOV can be obtained using Eq. (4). The radius of the IFOV is 15 pixels. The simulation platform is the MATLAB software. In the simulations, the target image is determined first. The light signal is quantitative; it is modulated and forms a light field, which is recorded. The detector receives the light field passing through the object and generates a bucket detector value. Multiple operations are performed according to the sampling number. The target image can be reconstructed by the correlation operation (Eq. (2)) for bucket detector values and light fields.

To quantitatively analyze and evaluate the quality of the reconstructed images, in this paper we use both subjective and objective evaluation methods. The subjective evaluation method is mean opinion score (MOS) [17], according to the visual perception to evaluate the quality of image. Image quality is divided into 5 grades, from good to bad. In the following formula, C_i is the image score of the ith grade, and N_i is the number of observers determining the level of the image.

$$C = \frac{\sum_{i=1}^{K} N_i C_i}{\sum_{i=1}^{K} N_i} \qquad (5)$$

The objective evaluation method is mean square error (MSE) [18], according to the following formula, where $x_{i,j}$ and $x'_{i,j}$ represent original and reconstructed image data respectively. The size of the image is $M \times N$.

$$MSE = \frac{\sum_{0 \le i < M} \sum_{0 \le j < N} (x_{i,j} - x'_{i,j})^2}{M \times N} \qquad (6)$$

4.1. Performance Comparison of RGI and GI

In GI, the laser is modulated by an SLM and speckle fields covering the whole object are generated, but the excessive range of light fields leads to the dispersion of energy. In RGI, a laser modulated by two reversed deflecting optical elements passes through the object along a rosette trajectory, and the light field is smaller and laser energy is concentrated. Simulations are carried out to verify the performance of RGI and GI, and MSE is used as the criterion to objectively evaluate the quality of the reconstructed image. Experimental results from Figs. 7 and 8 show that:
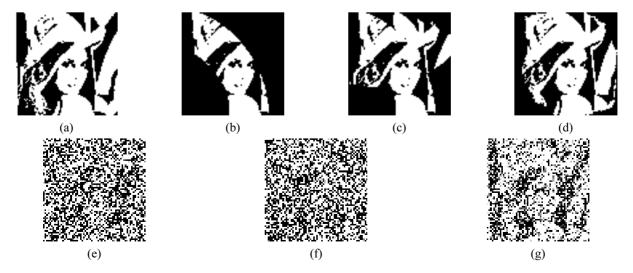

FIG. 7. (a) The test image. (b), (c), and (d) Reconstructed images for RGI with 50, 100, and 1000 samples respectively. (e), (f) and (g) Reconstructed images for GI, with 50, 100, and 5000 samples respectively.
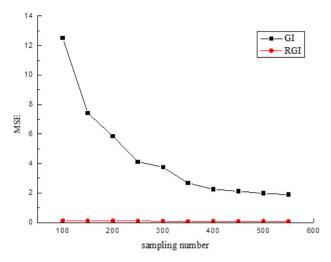
FIG. 8. Comparison of MSE for RGI and GI.

(1) The image reconstructed by RGI becomes more and more complete with increasing sampling number. When the sampling number is 1000, the reconstructed image is basically complete, but the margin is incomplete. The image reconstructed by GI has high noise under the same sampling number, and the object cannot be distinguished. When the sampling number is 5000, the object can be distinguished, but the reconstructed image still contains a lot of noise. Because RGI uses a smaller IFOV to collect the information about the object, compared to GI, the light field is small, the energy of the light source is more concentrated, and the energy received by the bucket detector is higher than in GI. Therefore, the reconstructed image effect of RGI is better than that of GI for the same number of samples.

(2) The image reconstructed by RGI does not contain noise, even when the sampling number is low, but the image reconstructed by GI contains a lot of noise. The object

transmissivity has a large effect on the noise. The more concentrated light source has a stronger response to the object's transmissivity, which is conducive to eliminating noise. In terms of noise removal, RGI is better than GI.

(3) At low sampling number, the MSE for RGI is smaller than for GI; this objectively illustrates that the image reconstructed by RGI is better than by GI. When RGI finishes a rosette scanning cycle, MSE values tend to be stable.

Therefore, compared to GI, RGI not only reduces the number of samples and improves the reconstruction efficiency, but also reduces the influence of noise and improves the quality of reconstruction.

4.2. Effect of Target Size on Time and Accuracy

In RGI, IFOV samples the image along the rose trajectory. The sampling density of the center is much higher than that of the margin, which causes the edge portion of the reconstructed image to be incomplete. Therefore, reconstruction of larger objects may not be ideal. A smaller object that is reconstructed by GI needs fewer samples than a larger object, but the reconstruction time is still long. The question of whether the size of the object will impact the reconstruction effect and reconstruction time in RGI should be answered through simulations. The center of the object is located at the center of a rosette trajectory. The PSNR of the reconstructed image is 30 as the standard, and the reconstruction time of GI and RGI are recorded.

Experimental results from Fig. 9 show that:

(1) Reconstruction time for RGI does not increase with increasing size of the object, and the reconstruction time is less than for GI. The reconstruction time for GI increases with increasing size of the object; the larger the object, the
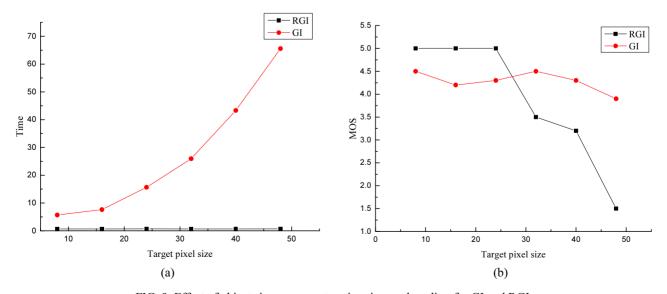

(a)

(b)

FIG. 9. Effect of object size on reconstruction time and quality, for GI and RGI.

longer the reconstruction time. RGI completes an image sampling needing one rosette scanning period; therefore, the sampling time is only related to the rosette scanning cycle, and the size of the object is irrelevant. So, compared to GI, RGI reduces the sampling time and improves the efficiency of reconstruction.

(2) If the reconstruction time is not considered, the image quality with RGI is better than with GI, when the object is smaller. When the object is bigger, the reconstruction quality of RGI is bad, while the reconstruction quality of GI remains steady. Its reconstruction quality is only affected by the edge area, though, and reconstruction quality of the central area is still obviously better than with GI. Because during sampling the reconstructed image is affected by the characteristics of rosette scanning, the sampling density of the center is much higher than that of the marginal area, and the quality of the reconstructed image is affected, but the quality of the central part of the image is good.

4.3. Effect of Different IFOVs on Reconstruction

Different IFOVs have great influence on the results of rosette scanning. Whether the size of the IFOV will affect the reconstruction effect in RGI should be verified through simulations. MSE is used as the evaluation criterion to objectively evaluate the quality of the reconstructed image.

The experimental results in Figs. 10 and 11 show that:

(1) Visual perception of the reconstructed image is enhanced with increasing size of the IFOV, because when a smaller IFOV scans the image, the reconstructed result has voids. When the IFOV is suitable, the image effect is good; only the lower-left corner of the reconstructed image is incomplete, as shown in Fig. 10(e). It shows that with an increase in the size of the IFOV, the image quality is gradually improved. The size of the IFOV can be calculated using Eq. (5); here the size of the IFOV is 8.2, consistent with the analysis in Fig. 11. This shows that the calculation method for IFOV in the rosette scanning system is also suitable for RGI, and when this IFOV scans the image, the reconstructed result is good.

(2) With increasing IFOV, the reconstructed image's MSE decreases gradually, but when the IFOV increases to a certain range, MSE begins to increase gradually. This is because an undersized IFOV affects image integrity, and an oversized IFOV affects the quality of the reconstructed image, causing redundant sampling. When the IFOV is
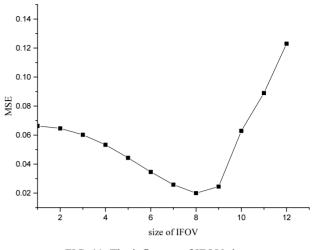

FIG. 11. The influence of IFOV size.

too large, energy is dispersed, and too much redundant sampling is not conducive to the correlation calculation, so the reconstruction is affected. Therefore, IFOV should be determined with Eq. (5), to not only cover the TFOV but also reduce redundant sampling, while having good anti-interference ability.

4.4. Effect of Different Positions of the Object on Reconstruction

In the process of sampling, the sampling density for the center is much higher than for the marginal area, which leads to an incomplete edge. To obtain a high-quality image, it is necessary to determine the effect of the object's position on the reconstruction results. This should be verified through simulations, with MOS as the evaluation criterion.

The experimental results from Figs. 12 and 13 show that:

(1) Reconstruction of the object in the central area is good, and the edge of the object is clear, but when the object is in the marginal area, the closer to the margin, the worse is the reconstruction, especially in a corner. This is because in RGI, the sampling density for the center is much higher than for the margin, so the quality of the reconstructed image of the center is good, while at the edge of the image the reconstructed image is incomplete, and the quality of image reconstruction is affected.

(2) The MOS curve shows that reconstruction is best when the object is in the center of the rosette trajectory.
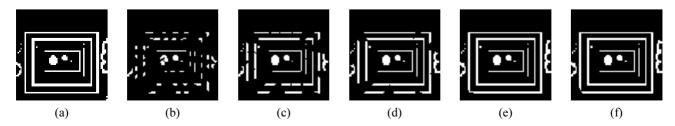

FIG. 10. Reconstructed image for different IFOVs. (a) Test image. In (b)-(f) the size of the IFOV is 2, 4, 6, 8, and 10 respectively.
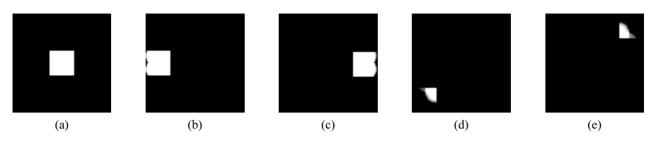
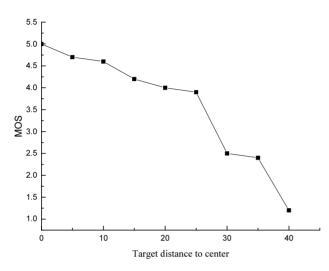FIG. 12. Reconstruction of an object at different locations.

FIG. 13. Evaluation of the reconstructed image at different distances from the center.

The more distance between the object and the central point of the rosette trajectory, the worse the reconstruction. Therefore, for an object located in the center of the TFOV, the reconstruction is good. If the object is located in the marginal area, a better reconstructed image is obtained by adjusting the position of the center of the TFOV.

The simulations indicate that RGI has an advantage over GI. RGI reduces sampling number, improves the quality of the reconstructed image, reduces the influence of noise on the image, and the size of the object does not affect the reconstruction time for the image. However, the size of the IFOV and the position of the object have a significant impact on reconstruction quality.

V. CONCLUSION

This paper presents a method for ghost imaging based on rosette scanning. The IFOV for rosette scanning is used to replace the light field, which is modulated by SLM, to sample the information of the scene. The scene can be completely sampled in one scan cycle. The effectiveness of this method is verified through numerical simulations, in which both subjective and objective evaluation methods are used to evaluate the quality of the reconstructed image. The simulation results show that RGI can reconstruct the image well with a low number of samples. Compared to traditional GI, RGI reduces energy loss and not only can improve the quality of the reconstructed image and reduce the influence of noise on reconstruction, but also reduces the sampling number and sampling time. However, this method also has some shortcomings: The sampling density for the center is much higher than for the edge of the TFOV. This shortcoming leads to the center of the reconstructed image being clear, but the edge being fuzzy.

REFERENCES

1. T. B. Pittman, Y. H. Shih, D. V. Strekalov, A.V. Sergienko, "Optical imaging by means of two-photon quantum entanglement," Phys. Rev. A **52**(5), R3429 (1995).
2. D. N. Klyshko, "Effect of focusing on photon correlation in parametric light scattering," Sov. Phys. **67**(6), 1131-5 (1988).
3. A. Gatti, M. Bondani, L. A. Lugiato, M. G. Paris, C. Fabre, "Comment on 'can two-photon correlation of chaotic light be considered as correlation of intensity fluctuations?'," Phys. Rev. Lett. **98**(3), 039301 (2007).
4. B. Yan-Feng, Y. Wen-Xing, and Y. Xiao-Qiang, "Noise analysis in ghost imaging from the perspective of coherent-mode representation," Chin. Phys. B **21**(4), 044206 (2012).
5. M. Zhang, Q. Wei, X. Shen, Y. Liu, H. Liu, J. Cheng, S. Han, "Lensless fourier-transform ghost imaging with classical incoherent light," Phys. Rev. A **75**(2), 021803 (2007).
6. X. H. Chen, Q. Liu, K. H. Luo, L. A. Wu, "Lensless ghost imaging with true thermal light," Opt. Lett. **34**(5), 695-697 (2009).
7. G. Brida, I. P. Degiovanni, G. A. Fornaro, M. Genovese, "Toward third order ghost imaging with thermal light," Int.

J. Quantum Inf. **9**(supp01), 341-348 (2011).

8. H. Wang and S. Han, "Coherent ghost imaging based on sparsity constraint without phase-sensitive detection," Europhys. Lett. **98**(2), 24003 (2012).

9. W. Gong and S. Han, "Correlated imaging in scattering media," Optics letters. **36**(3): 394-396(2011).

10. Y. Bromberg, O. Katz, and Y. Silberberg, "Ghost imaging with a single detector," Phys. Rev. A **79**(5), 053840 (2009).

11. J. H. Shapiro, "Computational ghost imaging," Phys. **78**(6), 1-2 (2008).

12. F. Ferri, D. Magatti, L. A. Lugiato, A. Gatti, "Differential ghost imaging," Phys. Rev. Lett. **104**(25), 253603 (2010).

13. R. P. Birchenall, M. A. Richardson, B. Butters, R. Walmsley, "Modelling an advanced ManPAD with dual band detectors and a rosette scanning seeker head," Infrared Phys. Technol. **55**(1), 67-72 (2012).

14. J. S. Choi, "Design of instantaneous field of view of the rosette scanning infrared seeker and dynamic simulation," Proc. SPIE - Int. Soc. Opt. Eng. **3365**, 158-168 (1998).

15. H. Uzeler and T. Aytaç, "Image reconstruction for single detector rosette scanning systems based on compressive sensing theory," Opt. Eng. **55**(2), 023108-023108 (2016).

16. H. Soltanizadeh and S. B. Shokouhi, "Increasing accuracy of tracking loop for the rosette scanning seeker using improved ISODATA and intelligent center of gravity," J. Appl. Sci. **8**(7), 1159-1168 (2008).

17. R. C. Streijl, S. Winkler, and D. S. Hands, "Mean opinion score (MOS) revisited: methods and applications, limitations and alternatives," Multimedia Syst. **22**(2), 213-227 (2016).

18. X. Q. Huang, J. S. Shi, J. Yang, and J. Yao, "Study on color image quality evaluation by MSE and PSNR based on color difference," Acta Photonica Sin. **36**(8): 295-298 (2007).